Journal of Electronic Imaging

JElectronicImaging.org

Context sensitive cardiac x-ray imaging: a machine vision approach to x-ray dose control

Stephen M. Kengyelics
Amber J. Gislason-Lee
Claire Keeble
Derek R. Magee
Andrew G. Davies

SPIE. IS&T imaging.org

Context sensitive cardiac x-ray imaging: a machine vision approach to x-ray dose control

Stephen M. Kengyelics,[a,*] Amber J. Gislason-Lee,[a] Claire Keeble,[a] Derek R. Magee,[b] and Andrew G. Davies[a]
[a]University of Leeds, Leeds Institute of Cardiovascular and Metabolic Medicine, Division of Biomedical Imaging, Worsley Building, Clarendon Way, Leeds LS2 9JT, United Kingdom
[b]University of Leeds, School of Computing, EC Stoner Building, Leeds, LS2 9JT, United Kingdom

Abstract. Modern cardiac x-ray imaging systems regulate their radiation output based on the thickness of the patient to maintain an acceptable signal at the input of the x-ray detector. This approach does not account for the context of the examination or the content of the image displayed. We have developed a machine vision algorithm that detects iodine-filled blood vessels and fits an idealized vessel model with the key parameters of contrast, diameter, and linear attenuation coefficient. The spatio-temporal distribution of the linear attenuation coefficient samples, when appropriately arranged, can be described by a simple linear relationship, despite the complexity of scene information. The algorithm was tested on static anthropomorphic chest phantom images under different radiographic factors and 60 dynamic clinical image sequences. It was found to be robust and sensitive to changes in vessel contrast resulting from variations in system parameters. The machine vision algorithm has the potential of extracting real-time context sensitive information that may be used for augmenting existing dose control strategies. *© 2015 SPIE and IS&T* [DOI: 10.1117/1.JEI.24.5.051002]

Keywords: cardiac; x-ray; contrast; machine vision.

Paper 15375SSP received May 14, 2015; accepted for publication Aug. 18, 2015; published online Sep. 21, 2015.

1 Introduction

In 2012, ischemic heart disease was the main cause of death worldwide, claiming an estimated 7.4 million lives.[1] Percutaneous coronary intervention (PCI) is an effective and minimally invasive treatment for cardiovascular disease resulting from a narrowing of coronary arteries. It works by mechanically improving the flow of blood to the heart.[2–4] The narrowing of the coronary arteries is caused by atherosclerosis, a build-up of fatty deposits, referred to as plaques, on the inner surface of the vessel wall. This may result in the heart muscle becoming starved of oxygen and nutrients, leading to chest pain or a heart attack, possibly causing permanent damage to the heart which may be fatal.

PCI procedures may involve several stages. These stages critically depend on the capability of x-ray and electronic imaging systems to adequately represent anatomical features, such that the clinical task can be achieved. Clinicians examine moving real-time images of the coronary arteries using an angiogram, where the blood vessels supplying the heart are made opaque to x-rays by injecting an iodine-based contrast agent into the vessel lumen. These are subsequently visualized using an x-ray detector and display. Ordinarily, images are acquired at 15 fps, resulting in sequences of anywhere between approximately 30 to 100 frames, though there is considerable variation.

The critical dependence on x-ray imaging during PCI procedures requires the use of ionizing radiation and it presents a concomitant hazard to both patients and staff.[5,6] Lowering radiation dose is advantageous, but any reduction may result in the deterioration of the diagnostic visual information that may compromise patient care.[7] The principle regulating x-ray dose to patients is to reduce it to a level that is as low as reasonably achievable. This so-called as low as reasonably achievable (ALARA) principle ensures that the radiation dose is sufficient to achieve the clinical task. In practice, this level is difficult to establish on an individual basis, as requirements differ by patient and task, and depend on the system geometry and settings employed.

The purpose of this paper is to propose a method to provide some contextual information that may be used to augment existing dose control strategies.

The contrast of iodine-filled blood vessels defines how well the vessel structures stand out from the surrounding anatomy. This is a key component for producing high-quality, diagnostically acceptable cardiac images. Notionally, the higher the level of contrast the better the vessels are visualized, leading to greater diagnostic utility that might be referred to as image quality in this context. The relationship of contrast in clinical images to the system parameters previously described is complex and is not discussed here. However, it is sufficient to note that currently cardiac imaging systems do not monitor or attempt to predict the level of image contrast in PCI procedures, despite being a key facet in producing clinically acceptable images.

A machine vision approach is investigated to detect iodine-filled blood vessels, to extract sample profiles orthogonal to their center lines, and to fit an idealized vessel model. Populations of contrast, vessel diameter, and linear attenuation coefficients are extracted. We show that the spatio-temporal distribution of the linear attenuation coefficient population, when appropriately arranged, can be described by a simple linear relationship despite the complexity of scene information. This relationship has the potential to

*Address all correspondence to: Stephen M. Kengyelics, E-mail: mrpsmk@leeds.ac.uk

provide real-time context-based image information that may be used to augment the existing automatic dose rate control (ADRC) strategy to deliver adequate image quality at the lowest radiation dose. Thus, the ALARA principle can be implemented on an individual basis.

2 Methodology

2.1 *Modification of Automatic Dose Rate Control*

Currently, most modern cardiac x-ray imaging systems regulate their radiation output by adjusting several system parameters to maintain a constant average output signal from the x-ray detector. The control system for the cardiac x-ray imaging unit, specific to this study, is illustrated in Fig. 1. The patient is positioned on a table, face-up, between the x-ray source and the detector. The source and detector are mounted on a gantry to keep the detector orthogonal to the central axis of the x-ray beam, and may be rotated around the patient from left to right, and from head to toes, to produce different projections. The table height and source-to-detector distance may also be adjusted independently of the gantry projection angles. These degrees of freedom allow the positioning of the equipment to optimize the view of the clinical feature of interest, or to sequentially obtain multiple views of the same feature from different angles. Referring to Fig. 1, if the average output of the x-ray detector decreases with respect to that requested by the system mode selection, a difference signal is generated and used to calculate a new set of system parameters that will increase the output of the x-ray source to reduce the difference signal to zero. The system parameters calculated are the x-ray tube voltage (kVp), current (mA), and pulse width (ms). The average output of the detector is calculated per image frame using the digital values contained within a predefined circular measuring field. Overall, the system is designed to maintain a constant average detector signal, irrespective of variations in patient anatomy and system geometry, up to the point where statutory stipulations limit any further increase in the x-ray radiation output.

While this form of ADRC scheme is effective, it does not provide any information derived from the available image data. We propose to modify the feedback control scheme shown in Fig. 1 by using real-time image information to augment the existing feedback control loop.

2.2 *Image Information Extraction*

The contrast of iodine-filled vessels is defined here according to Eq. (1), where s is the peak digital value of the profile of the vessel cross section and b is the average digital value of the profile outside the extent of the vessel. Referring to Fig. 2, x-ray photons penetrating the patient form a digital image of the vessel and the background anatomy. Contrast is measured according to our definition from a profile $P(x)$ extracted from the image that is orthogonal to the center-line of the vessel, where x is the displacement in pixel units. The profile is defined to overlap either edge of the vessel by one-half of the vessel diameter. The definition assumes a linear relationship between the recorded digital value and incident x-ray photon fluence.

$$C = \frac{s - b}{b}. \tag{1}$$

There are a number of challenges in obtaining useful measurements of iodine-filled coronary arteries from angiograms to augment current ADRC strategies. During image sequence acquisition, the scene is continuously changing due to the inflow and outflow of contrast agent, cardiac motion, respiratory, and minor patient movement. In some instances, there is movement of the entire patient, as the clinician repositions them to optimize the view. Due to this dynamic nature and with the presence of multiple, often

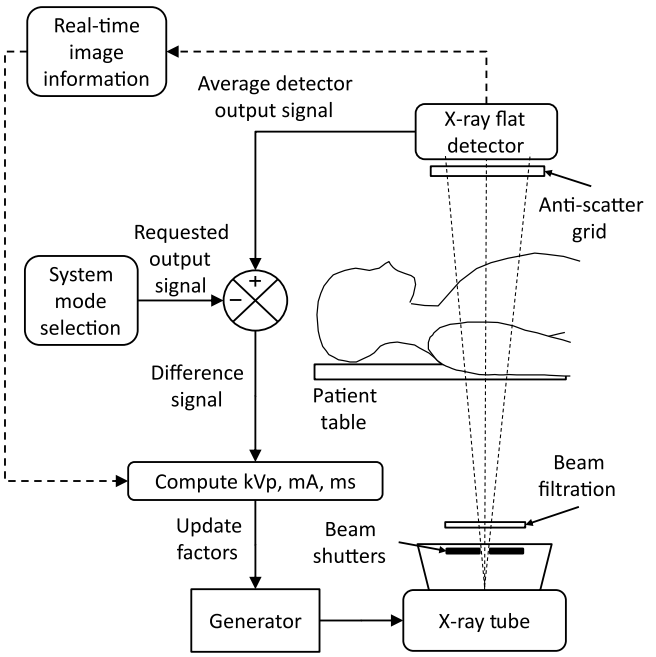

Fig. 1 Cardiac x-ray imaging system: feedback control diagram.

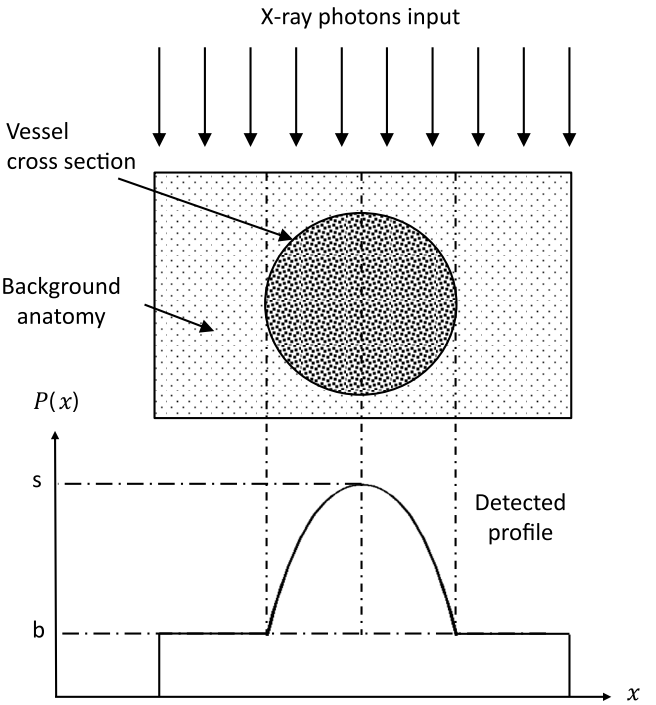

Fig. 2 Detected profile of blood vessel filled with contrast agent.

overlaying, vessel structures, it is not currently possible to detect and reliably segment complete coronary artery networks. In addition, coronary artery trees are composed of vessels with a range of different diameters, thus single measurements would be of limited value, since larger vessels will produce higher contrast just by virtue of containing more x-ray attenuating material. For such measurements to be useful, it would also be necessary to relate them to the vessel width and track the exact point where the measurement was made from frame to frame. It is possible to detect, segment, and measure the diameters of sections of vessel in individual image frames, but it is difficult to define a particular location on a vessel that might be reidentified on a subsequent image frame. This is due to the dynamic nature of the scene described above.

Our approach avoids these problems by not attempting to fully segment the coronary artery tree or identify individual features from frame to frame. Instead, partial segmentation and morphological operations are used to identify multiple points representing the center-lines of vessel segments for a range of vessel diameters. These are remote from bifurcations and are not overlaying any complex anatomical structures. Using these points, cross-sectional profiles are extracted that are orthogonal to the length of the vessel. A simple model of a tubular blood vessel filled with a contrast agent is fitted to each profile. The key parameters of the model are the vessel diameter, contrast, and linear attenuation coefficient.

These parameters may be viewed as referred values, in that it is assumed they would result from measuring an idealized circular vessel. This idealized vessel has its long axis imaged in a geometric plane parallel and immediately adjacent to the detector face, and orthogonal to a monoenergetic x-ray source, regardless of its displacement in the image field. In practice, this assumption is not true for a number of reasons. For example, a blood vessel may be orientated such that it is foreshortened with respect to the detector, resulting in a higher contrast value. However, the foreshortened vessel would appear darker to an observer compared to the same vessel that was not foreshortened. Hence, despite not having an accurate contrast value for the vessel, if it were ideally imaged, the referred contrast offers practical values that are related to contrast presented to the user.

The parameters for all cross-sectional profiles form a population of values both spatially, across the extent of a single frame, and temporally from frame to frame. The referred contrast and diameter parameters are useful metrics relating to observer perception. The linear attenuation coefficients are more useful in reflecting changes in the concentration of the contrast agent or variations in the system settings, such as the x-ray beam energy or the number of scattered x-ray photons incident on the detector.

In addition, the population of linear attenuation estimates, when appropriately arranged, was found to have a linear relationship over the majority of values contained in an image frame. This relationship provides a simple categorization of the linear attenuation coefficients for a single image frame as a whole. It is also found to be relatively stable from frame to frame, and as such has the potential to provide context sensitive feedback to augment the ADRC, despite the complexity of the scene.

2.3 *Data Acquisition*

Digital image sequences were obtained from a modern cardiac x-ray imaging system, used routinely for PCI procedures in the Leeds General Infirmary, United Kingdom (Allura FD10, Philips Healthcare).

The sequences were acquired prior to the application of any nonlinear image processing algorithms via a propriety data capture device installed by the manufacturer. The only processing applied prior to capture was linear scaling and a dynamic range compression look-up table. Both test phantom and clinical images were acquired. Each image sequence contained approximately 30 to 50 image frames of 1024×1024 pixels.

Test images were acquired using an anthropomorphic chest phantom (Radiology Support Devices, Alderson Phantoms, Long Beach) containing a left coronary artery (LCA) filled with contrast agent. The phantom was arranged on the examination table in a posteroanterior projection, and the heart positioned at the isocenter, the center of rotation of the x-ray tube and detector. This was prior to angulation of the gantry to optimize the view of the coronary arteries. An air gap of 10 cm was set between the exit surface of the phantom and the entrance to the detector, reflecting clinical practice. The 15-cm field size was selected and a series of images of the LCA were acquired at peak x-ray tube voltages of 50, 70, 90, and 110 kVp, using the digital-acquisition mode. Approximately 50 image frames per sequence were acquired. Adjustment of the kVp, mA, and ms was manually performed by over-riding the ADRC. This series provided static images with the same geometrical arrangement of the LCA, but with decreasing contrast values due to the increase in kVp.

Clinical images came from different patient examinations, and comprised 30 LCA and 30 right coronary (RCA) sequences, acquired at 15 fps, using the digital-acquisition mode and a 15-cm field size. The image sequences chosen did not contain any additional catheters, guide wires, or other surgical devices other than the main catheter used to introduce the iodine contrast agent.

2.4 *Measurement Algorithm Description*

A machine vision algorithm was developed in MATLAB®[8] and can be divided into two broad operations: (1) candidate vessel location and (2) vessel parameter estimation.

2.4.1 *Candidate vessel location*

This section of the algorithm returned coordinates of candidate points within a single image frame which are on the center-lines of iodine-filed coronary arteries, and within a specified range of diameters and lengths in the image plane. The algorithm is applied to all image frames in a sequence.

The major steps of this section of the algorithm are shown in Table 1.

Step 1.1: Extract active image region: the raw data sequences contained dark regions at their periphery produced by the x-ray shuttering that is used to restrict the irradiation of the patient to only those areas of clinical interest. For the image sequences in this study, the edges of the shutters produce penumbral effects in the image plane at the interface of the clinical image information.

Table 1 Candidate vessel location: list of algorithm steps.

Step	Brief description
1.1	Extract active image region
1.2	Reverse system compression
1.3	Apply Frangi filter
1.4	Generate mask image
1.5	Clean mask image
1.6	Create skeleton image from mask
1.7	Remove branches
1.8	Remove small skeleton sections
1.9	Generate list of coordinates
1.10	Subsample list of points
1.11	Return list of candidate points

This is due to their position close to the finite sized x-ray source. The resulting penumbra can be misidentified as vessel structures; so prior to further analysis, the clinical image data are extracted from inside the region defined by the shutters.

The vertical shutters were identified by averaging the pixel values in the vertical direction to form a profile that has a length equal to the width of the image. The profile is smoothed, differentiated, and a threshold applied to identify the edges of the shutters which generally produce the two largest gradients in the image. Occasionally, other structures contained in the active image area can produce high gradients, such as surgical instruments or devices. However, the shutters can be identified as they work as a pair, closing from the periphery of an image to the center, so spurious edges may be easily identified. Identification of the horizontal shutters was performed in the same way but in the orthogonal direction. Having identified vertical and horizontal shutter positions, the active image area was extracted from the image frame.

Step 1.2: Reverse system compression: the digital values were transformed using a look-up table to invert the dynamic range compression applied by the imaging system prior to data capture. This restored a linear relationship between increments of the input x-ray exposure and digital values.

Step 1.3: Apply Frangi filter: a Frangi filter[9] was applied to the image sequence at five different scales to cover the vessel sizes of interest. The filter identifies tube-like structures within an image at specified scales. The algorithm returns a number of responses, including a direction image that contains the orientation of the eigenvectors for all scales.

Step 1.4: Generate mask image: a binary mask image of the detected vessel locations was generated by applying a threshold to a standard deviation map of the direction image for local regions of interest of 3×3 pixels. Generally, the eigenvectors in the local vicinity of a vessel will all have similar values. Therefore, they will have a low standard deviation in comparison with other structures not resembling vessels. The use of the direction image, as opposed to the scale response image, was chosen to generate the mask. This is because it is also required later for calculating the direction of profiles orthogonal to the vessel center-lines, and is more computationally efficient.

Step 1.5: Clean mask image: noise was removed using standard morphological operations. An example of a binary mask derived using steps 1.1 to 1.5 for a single frame of an LCA sequence, Fig. 3(a), is shown in Fig. 3(b).

Step 1.6: Create skeleton image from mask: a skeleton was produced by thinning the mask image as shown in Fig. 3(c).

Step 1.7: Remove branches: bifurcations in the mask and regions around them are removed, as only measurements across single unobstructed sections of vessel were of interest, see Fig. 3(d).

Step 1.8: Remove small skeleton sections: the length of each section of skeleton was calculated and lengths below 30 pixel units were not included in the analysis.

Step 1.9: Generate list of coordinates: any nonzero points in the resulting skeleton image represent candidates for the center-lines of vessel segments. An ordered set of coordinates of nonzero points were generated per vessel, such that the first and last points for each vessel corresponded to the start and finish of the vessel. Intermediate points were sequentially sorted according to their position along its length between the start and the finish points.

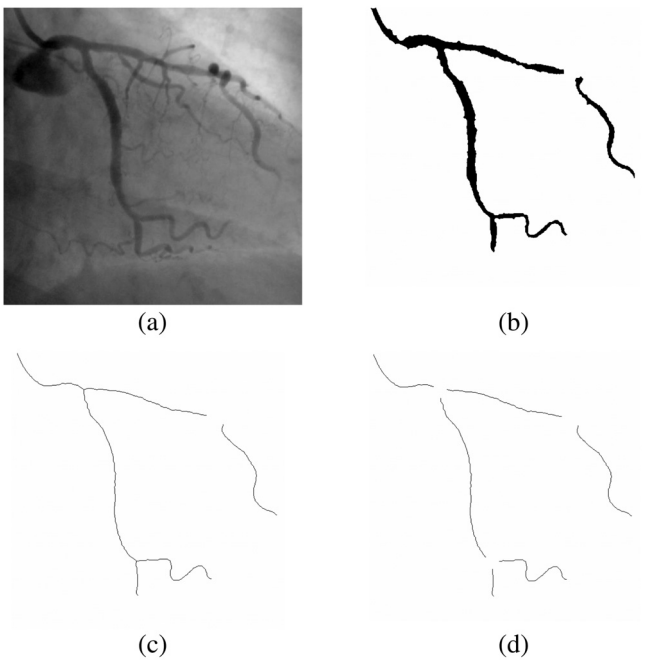

Fig. 3 Candidate vessel location: (a) left coronary artery (LCA) single frame, (b) binary mask, (c) skeleton, and (d) skeleton with bifurcations removed.

Step 1.10: Subsample list of points: the user may subsample the list of candidates by retaining every nth point, as not all points are required to obtain a good representation of the contrast distribution along a vessel.

Step 1.11: Return list of candidate points: return the coordinates of candidate points for each vessel within each frame.

2.4.2 *Vessel parameter estimation*

This part of the algorithm returned estimates of the vessel parameters such as contrast, vessel diameter, and linear attenuation coefficient. The estimates were associated with each valid candidate point returned using the algorithm in Sec. 2.4.1, by fitting an idealized vessel profile model orthogonal to the center-line.

The major steps of this section of the algorithm are shown in Table 2.

Step 2.1: Determine the vessel direction: the orientation of the long axis of the vessel at the location of the candidate point is determined from the Frangi direction image.

The overall aim of steps 2.2 to 2.7 is to extract a profile P between two points $[P_1, P_2]$. The line between the points is orthogonal to the center-line of the vessel and overlaps it by one-half of the vessel diameter D.

Table 2 Vessel parameter estimation: list of algorithm steps.

Step	Brief description
2.1	Determine the vessel direction
2.2	Estimate location of two points orthogonal to vessel direction on either side
2.3	Skip pairs of points if either is outside image
2.4	Use points to estimate vessel diameter **D** from mask image
2.5	Re-estimate location of points orthogonal to vessel using (1) and (4)
2.6	Extract profile, **P** between pairs of points from (5)
2.7	Calculate $\mathbf{V_1}$ and $\mathbf{V_2}$-the location of the upper/lower limits of the vessel in **P**
2.8	Fit linear curve to **P** using points outside the region of the vessel
2.9	Skip profiles exceeding defined gradient limit
2.10	Subtract the curve fit from **P**
2.11	Normalize the result to unity yielding $\mathbf{P_N}$
2.12	Fit the vessel model to $\mathbf{P_N}$ using start values $\mathbf{P_c}$ and **D**
2.13	Skip profiles that produce a goodness-of-fit outside defined limit
2.14	Return contrast, vessel diameter, and linear attenuation coefficient estimates

The points are also equally spaced on either side of a candidate center-point P_c, as illustrated in Fig. (4). The overlap provides a consistent approach to considering the contrast of different sized vessels to that of the surrounding image content.

Step 2.2: Estimate the location of two points orthogonal to vessel direction on either side: initially, the diameter of the vessel is not known, so a guess is made for two points. These points are equally spaced on either side of the candidate point at a distance of 20 pixel units, and orthogonal to the direction determined in step 2.1. The placement of these points allows for the largest vessel size accommodated by the scales initially set for the Frangi filter.

Step 2.3: Skip pairs of points if either is outside the image: inevitably, some candidate points close to the edge of an image will generate points from step 2.2 that are outside the image, and therefore, are excluded from the analysis.

Step 2.4: Use points to estimate vessel diameter D from mask image: a binary image is created that represents the two points generated from step 2.2 and all the points in a straight line between them. This image is logically multiplied with the mask generated in steps 1.1 to 1.5. The distance between the endpoints of the resulting profile represents an estimate of the vessel diameter D, orthogonal to the candidate center-line point.

Step 2.5: Re-estimate locations of the two points orthogonal to the vessel using the vessel direction image from step 2.1, and the estimate of the vessel diameter from step 2.4.

Step 2.6: Extract profile, P between the pair of points, assigned to be $[P_1, P_2]$, generated in step 2.5.

The purpose of steps 2.7 to 2.10 is to remove trends from P associated with background anatomy, as illustrated in Fig. 5, to provide an average single background level for the contrast estimation. A linear curve fit is applied to the regions of the vessel profile on either side of the vessel and then subtracted from the profile.

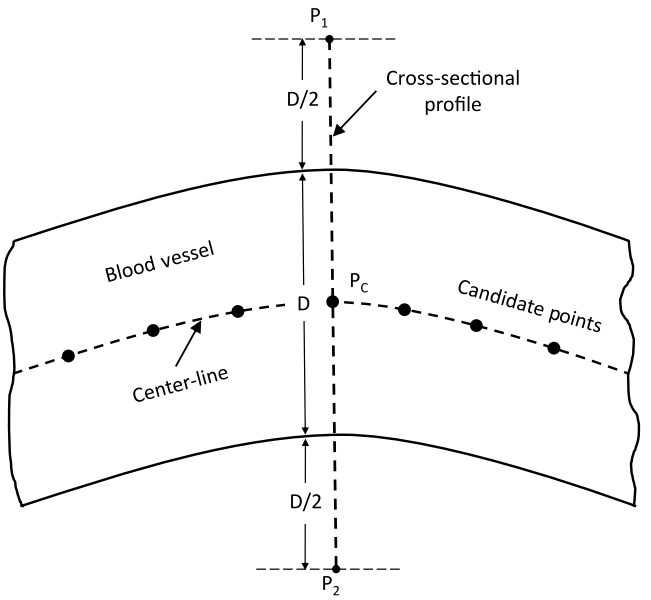

Fig. 4 Cross-sectional profile location.

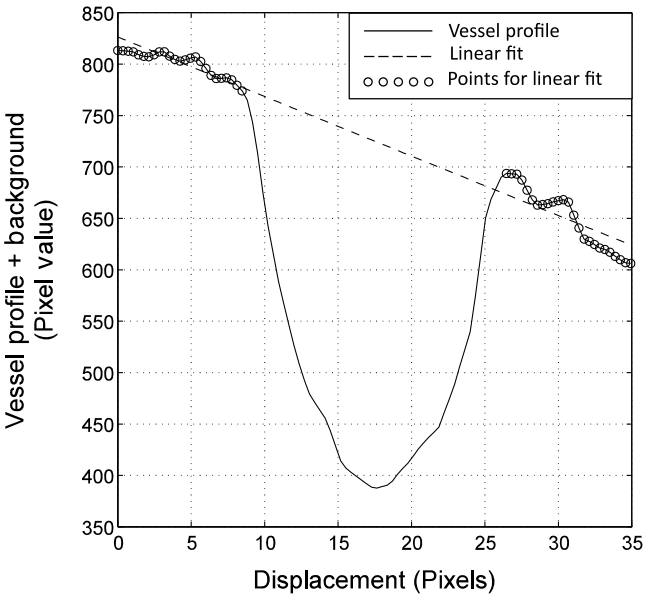

Fig. 5 Example of background trend removal from the vessel profile.

The result is then inverted and normalized to a form suitable for the ideal vessel model fitting, as shown in Fig. 6.

Step 2.7: Calculate V_1 and V_2: the location of the limits of the vessel in P: these values are calculated from the vessel width estimate and the candidate center-line point position: $V_1 = P_c - D/2$ and $V_2 = P_c + D/2$.

Step 2.8: Fit linear curve to P using points outside the region of the vessel: the regions of support for the linear curve fit are in the ranges P_1 to V_1 and V_2 to P_2.

Step 2.9: Skip profiles exceeding defined gradient limit: extreme gradients (>30) indicate the presence of either another vessel, or possibly part of a medical device in the vicinity, and are excluded from the analysis.

Step 2.10: Subtract the curve fit from P.

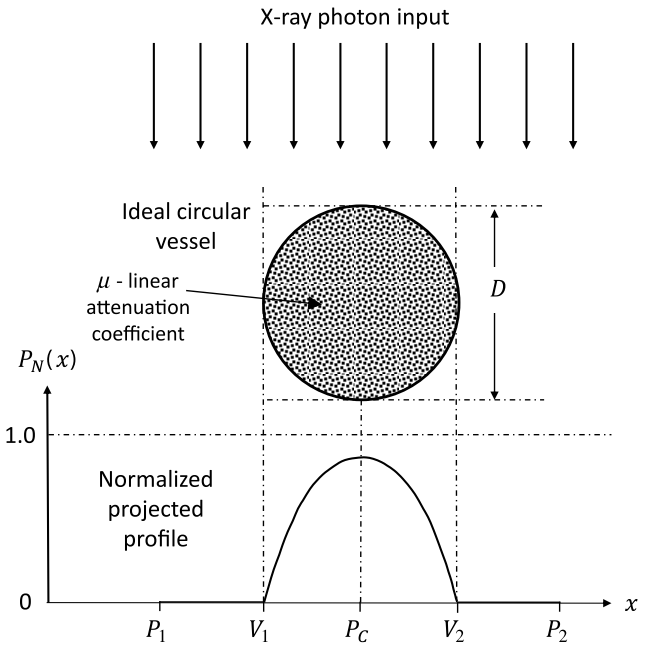

Fig. 6 Normalized cross-sectional profile.

Step 2.11: Normalize the result to unity yielding P_N: normalize the result according to Eq. (2), where x is the displacement in pixel units, and $P_{\max}$ is the maximum value of the profile P.

$$P_N(x) = 1 - \frac{P(x)}{P_{\max}}. \tag{2}$$

The purpose of steps 2.12 to 2.14 is to fit an idealized vessel profile model to P_N and return the parameters such as contrast, vessel diameter, and linear attenuation coefficient. The vessel model is derived by calculating the cross-sectional profile of the attenuation of an ideal circular blood vessel. This ideal vessel is filled with a contrast agent with a linear attenuation coefficient μ, and imaged using a monoenergetic, parallel beam x-ray source, together with an ideal detector, as illustrated in Fig. 6.

The vessel model is given by Eq. (3), where $\mu_n = \mu/D$ is the linear attenuation coefficient normalized to the vessel diameter.

$$P_M(x) = \begin{cases} 1 - e^{-\mu_n D}\left|\cos\left[\frac{\pi}{D}(x - P_c)\right]\right| & x \in [V_1, V_2] \\ 0 & \text{elsewhere.} \end{cases}, \tag{3}$$

μ_n is used in the vessel model so that the amplitude and width of the response can be independently set for the fitting algorithm to more easily converge, then μ is returned once fitting is complete. Contrast is the maximum value of $P_M(x)$. Note that μ is expressed per pixel unit. Conventionally, the linear attenuation coefficient is a material-specific constant that describes the fraction of a narrow beam of monoenergetic x-rays that are absorbed or scattered, per unit thickness. Image contrast arises due to differences in the thickness and linear attenuation coefficients of a material, and the structures surrounding it. Here, we model the measured contrast profile arising from an ideal circular vessel, filled with some material of linear attenuation coefficient μ, that accounts for the measured diameter and contrast of the vessel with respect to its local background.

Step 2.12: Fit the vessel model to P_N using start values P_c and D: a nonlinear least-squares Levenberg–Marquardt algorithm is used to fit P_N in the region of support between the points V_1 and V_2. An example of the model fit of the profile of an iodine-filled blood vessel is shown in Fig. 7. The start values, together with the use of μ_n, greatly reduce the number of iterations required for the algorithm to converge.

Step 2.13: Skip profiles that produce a goodness-of-fit outside the defined limit: profiles resulting in a mean-squared-error of greater than 1×10^{-3}, calculated within the region of support when fitted to the model, are excluded from further analysis. The mean-squared-error is a scalar estimate of the variance of the error term of the model.

Step 2.14: Return the contrast, vessel diameter, and linear attenuation estimates.

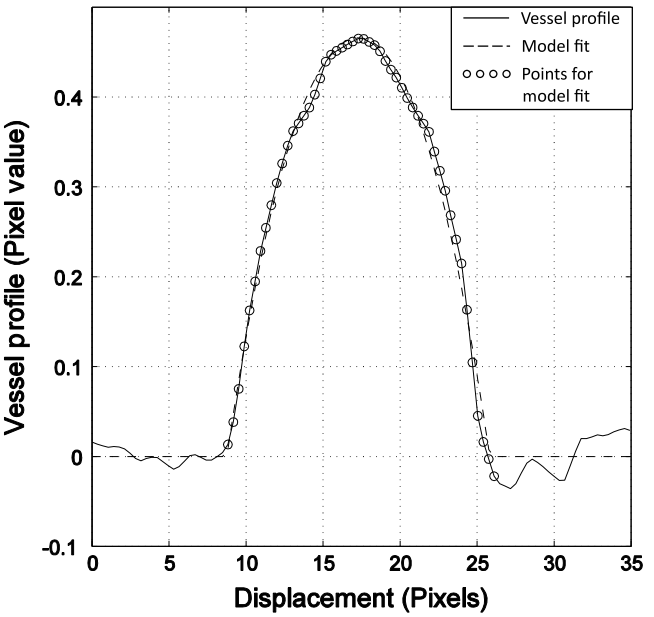

Fig. 7 Example of ideal vessel model fit to measured cross-sectional profile.

2.5 *Data Normalization*

The population of samples for the linear attenuation coefficients for each image frame are sorted from lowest to highest values. They are then arranged against an axis of sample rank normalized to the number of samples, as illustrated in Fig. 8, for a single frame from an LCA sequence. This normalization of the abscissa allows the intercomparison of the values on a common scale from frame to frame and sequence to sequence. Note that over the region [0.1,0.75], the relationship is approximately linear for this sequence. This was found to be true for all LCA and RCA images contained in the 60 clinical test sequences for a region [0.25,0.75].

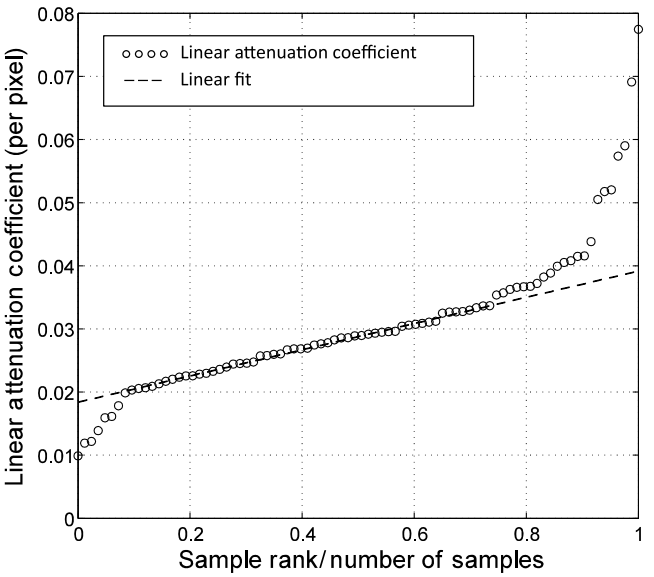

Fig. 8 Linear attenuation coefficients: data normalization.

2.6 *Algorithm Testing*

The purpose of developing the automatic measurement algorithm was to estimate the parameters (contrast, diameter, and linear attenuation) of iodine-filled vessels, over a significantly representative extent of the coronary artery tree. As such, the algorithm need not identify all the vessels present. It should, however, measure the contrast values with a precision comparable with a manual measurement technique. Hence, two test criteria were defined. First, if present, the algorithm must automatically locate a minimum of 75% of the length of one section of iodine-filled coronary artery in every image frame of a sequence. Second, the measurement of contrast must be within 5% compared to an appropriate manual measurement technique.

The first criteria were tested by running the algorithm on the 60 clinical test image sequences. Each sequence was then displayed to a user a single frame at a time. The positions of iodine-filled coronary arteries identified by the algorithm were overlaid as colored contour lines on the display, along with a numeric graticule. The user recorded the approximate total length of the longest vessel, either fully or partially identified by the algorithm, and the length of the identified portion of that vessel.

For the second criteria, the algorithm was used to measure the contrast level of single sections of iodine vessel. The regions of interest were 100×100 pixels, from a single image frame, extracted from each of 60 test sequences. For each image, the algorithm automatically located the vessel, estimated the center-line, performed the model curve fit, and calculated the contrast at all the sample points along its length. The contrast results (around 30 to 50 in each region) were then averaged for all the sample locations within the bounded area.

For each of the regions of interest, the vessel contrast was measured using a manual technique. Ten sample locations along the vessel center-line were used and the results averaged. The manual technique used a software-based measurement tool that allows a user to position lines and markers on the image frames displayed on-screen. Profiles could also be generated and measured against numeric scales. For each image, the user marked the edge of the vessel boundary by inspection, and then defined a center-line equidistant from each boundary. Ten equally spaced sample points were marked along the center-line within the bounded region of interest, and orthogonal profiles were generated at these locations. The profile values were transformed according to Eq. (2) and displayed as a graph of contrast against displacement. The user estimated the peak contrast level from an overlaid numerically labeled graticule.

The sensitivity of the algorithm to variations in the attenuation coefficient of the contrast agent was tested. Testing consisted of applying it to the series of chest phantom images acquired at a range of kVp values, as described in Sec. 2.3.

The temporal behavior of the algorithm to variations in the cardiac image scene from frame to frame was also tested. The referred linear attenuation coefficient at the normalized abscissa value of 0.5, known as the midvalue, see Fig. 8, was assessed as a function of frame number for three clinical image sequences.

3 Results

For the first test criteria, the algorithm successfully located a minimum of 75% of the length of one section of iodine-filled

coronary artery if present. This was true for every image frame of a sequence, for the 60 test image sequences examined.

In the second test criteria, the standard deviation for all contrast measurements was less than 0.05. This indicated good reproducibility for both measurement methods, and also supported the assumption that the profile of the vessel did not significantly change over the small predefined regions of interest.

Recall that the population of samples for the linear attenuation coefficients, as illustrated in Fig. 8, is approximately linear in the region [0.1,0.75] of the x-axis for all 60 image sequences. This relationship provides a simple categorization of the linear attenuation coefficients for a single image frame as a whole, despite the complexity of the scene. The departure from a linear relationship below this range is thought to be due to the partial filling of some of the blood vessels with contrast agent. Above this range, it is thought to be due to foreshortening of some of the vessels as they wrap around the heart.

Figure 9 shows a Bland–Altman plot comparing the automatic and manual measurement methods, indicating a mean bias of 0.001. The 95% confidence limits −0.046 to 0.048 are approximately what would be expected from the standard deviation of the individual measurements.

Figure 10 shows the linear attenuation coefficients for anthropomorphic chest phantom images. It demonstrates that the measurement algorithm is sensitive to variations in linear attenuation coefficient, resulting from changes in the x-ray system settings.

Figure 11 shows the referred mid-value linear attenuation coefficients as a function of frame number for three LCA clinical image sequences. The sequences were chosen as they shared similar system geometry and displayed anatomy, and only differed significantly in the kVp value. These results show that the mid-value linear attenuation coefficient is stable over time. This is despite the variation of scene information resulting from the transit of contrast agent and complex movement of the heart. The larger deviation

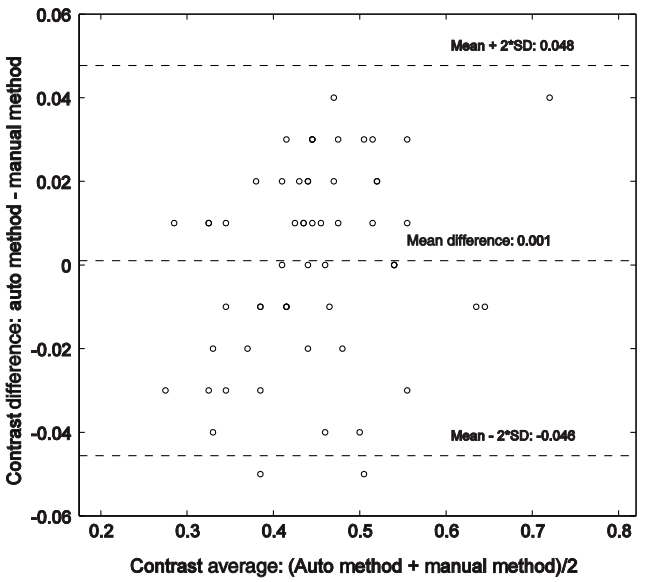

Fig. 9 Bland–Altman plot comparing the machine vision algorithm with a manual measurement technique.

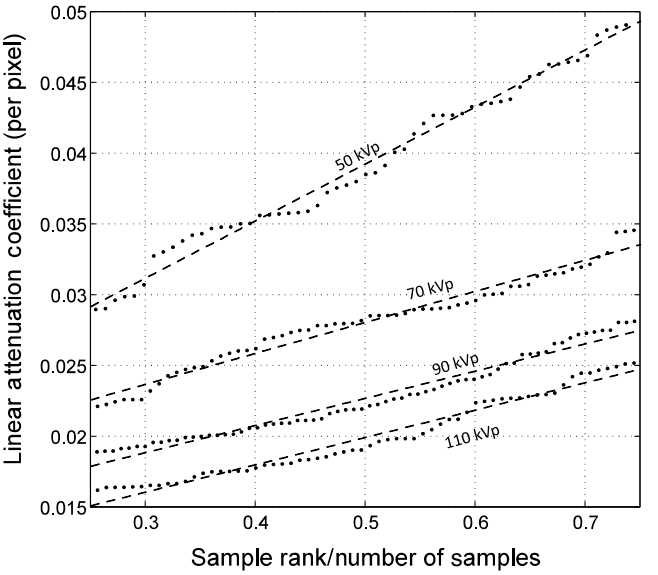

Fig. 10 Attenuation coefficients for an anthropomorphic chest phantom.

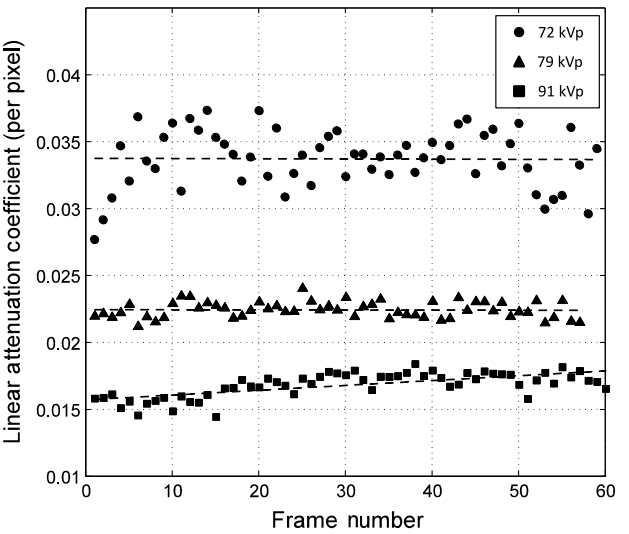

Fig. 11 Attenuation coefficients for clinical image sequences as a function of frame number.

observed for 72 kVp values is due to some of the vessels moving over background anatomical features, from one image frame to the next, which have different attenuation characteristics.

4 Discussion and Conclusions

We have developed an automatic machine vision algorithm to parametrize the contrast in iodine-filled coronary arteries. The overall aim was to provide context sensitive imaging information for use in the dose control feedback system of a modern cardiac imaging system.

Contrast is not the only important aspect of image quality for cardiac imaging. Image noise, spatio-temporal resolution properties, and the application of specialist image processing are also critically important. We selected contrast for our initial investigation, as the x-ray imaging system has several convenient degrees of freedom by which to influence it.

These include the x-ray tube voltage (kVp), x-ray beam filtration, the source-to-detector distance (which influence scatter and, therefore, contrast), and the antiscatter grid.

The algorithm was required to identify a representative sample of vessels across the coronary artery tree in each image frame. It was also need to make estimates of contrast, diameter, and linear attenuation coefficients for an idealized vessel model along the length of identified vessels. The results presented have demonstrated that both requirements have been met for the 60 clinical image sequences tested. The algorithm is computationally inexpensive and has the potential of working in real time. In addition, it has been demonstrated that the algorithm is sensitive to changes in system settings that directly affect the linear attenuation coefficient of the contrast agent. It also provides a robust measurement over time even in the presence of variable scene information.

Future work will incorporate the referred linear attenuation information into the dose control feedback loop for a modern cardiac x-ray imaging system. In addition, the contrast results will be compared to an observer experienced with interpreting images, concerning the perceived contrast and acceptability of images, to achieve a clinical objective.

Acknowledgments

This work has been performed in the project PANORAMA, funded by grants from Belgium, Italy, France, the Netherlands, United Kingdom, and the ENIAC Joint Undertaking.

References

1. World Health Organization, "The top 10 causes of death. The 10 leading causes of death in the world, 2000 and 2012," 2014, http://www.who.int/mediacentre/factsheets/fs310/en/# (17 June 2014).
2. P. Ludman, *National Audit of Percutaneous Coronary Interventional Procedures Public Report*, British Cardiovascular Intervention Society, London, England (2011).
3. E. Grech, "Percutaneous coronary intervention. I. History and development," *Brit. Med. J.* **326**, 1080–1082 (2003).
4. E. Grech, "Percutaneous coronary intervention. II. The procedure," *Brit. Med. J.* **326**, 1137–1140 (2003).
5. M. J. Eisenberg et al., "Cancer risk related to low-dose ionizing radiation from cardiac imaging in patients after acute myocardial infarction," *Can. Med. Assoc. J.* **183**(4), 430–436 (2011).
6. D. Žontar et al., "Patient peak skin doses from cardiac interventional procedures," *Radiat. Prot. Dosimetry* **139**, 162–165 (2010).
7. A. J. Gislason-Lee, A. R. Cowen, and A. G. Davies, "Dose optimization in cardiac x-ray imaging," *Med. Phys.* **40**, 091911 (2013).
8. MATLAB, *Version 8.3.0.532 (R2014a)*, The MathWorks Inc., Natick, Massachusetts (2014).
9. A. Frangi et al., "Multiscale vessel enhancement filtering," *Lec. Notes Comput. Sci.* **1496**, 130–137 (1998).

Stephen M. Kengyelics received his MSc degree in physics from the University of Leeds, United Kingdom, in 1997. He received his BEng degree in electrical and electronic engineering from the University of Plymouth in 1991. His research has included quantifying the performance of medical x-ray image detectors and the application of machine vision to interventional cardiac x-ray imaging.

Amber J. Gislason-Lee is a medical physicist based at the University of Leeds, United Kingdom. She received her BSc degree from the University of Winnipeg, Canada, and her MSc degree in medical physics from the University of Leeds. Her research has included pediatric dose optimization in diagnostic radiology and quantifying performance of cardiac flat-panel detector-based interventional x-ray imaging systems.

Claire Keeble received her MSc degree in statistics from the University of Leeds, United Kingdom, in 2011 and she received her BSc degree in mathematical studies there in 2010. She has since worked between the School of Mathematics and the School of Medicine at the university, applying and developing statistical methodology for use in medical research.

Derek R. Magee is a lecturer in computer science at the University of Leeds, United Kingdom. He received his PhD from the University of Leeds in 2001 and his BSc degree in engineering from Durham University in 1995.

Andrew G. Davies is a lecturer in medical imaging at the University of Leeds, United Kingdom, where he received his MSc degree in medicine in 1995 and his BSc degree in computer science in 1990. His research interests include image quality, system performance, and optimization of medical x-ray imaging systems.